CONF-850310--97

DE85 011559

ASSESSMENT OF MAGNETIC FIELD ASYMMETRIES IN ELMO BUMPY SQUARE*

T. UCKAN and N. A. UCKAN
Oak Ridge National Laboratory
Oak Ridge, Tennessee 37831
(615) 574-1354

ABSTRACT

There exist two separate and independent magnetic field asymmetries in the ELMO Bumpy Square (EBS). One is associated with the small perturbations in the magnetic field, known as the field errors, caused by coil misalignments during installation, imperfection in coil winding, etc. The second source of asymmetry is the magnetic field ripple in the high-field toroidal solenoids (corners) produced by the finiteness of the number of coils. In general, these two sources of asymmetry introduce enhanced transport losses (in addition to other effects) to the system, although they affect different classes of particles. Toroidally passing (circulating) particles ($v_\parallel/v \sim 1$) are influenced by the field errors, whereas trapped particles ($v_\parallel/v \sim 0$) in the corners are influenced by the field ripple. In this paper we discuss these two effects separately and calculate the allowable magnitudes of the field error and field ripple in EBS, both for an experimental-size device and for a reactor.

INTRODUCTION

The ELMO Bumpy Square (EBS) geometry consists of linear segments of simple mirrors that are linked by sections of high-field toroidal solenoids (corners) as shown in Fig. 1. In this configuration the toroidal effects are localized in the corners.[1,2]

An ideal EBS is a closed field line configuration with zero rotational transform and no toroidal current, characteristics of an ideal ELMO Bumpy Torus (EBT). This current-free equilibrium configuration is very sensitive to the system magnetic field asymmetries (field errors). If large enough, these field errors ($\delta B/B$) can cause field lines to spiral out of the confinement volume (enhanced losses), thereby degrading confinement.[3,4] In practice, the field errors can arise from many different sources: coil misalignment, imperfect coil winding, the presence of nearby magnetic materials, etc. In this paper we discuss only the first error source and estimate the maximum tolerable field error ($\delta B/B$) and, in turn, the corresponding constraint imposed on the alignment of the coils.

ORNL-DWG 84-2753A FED

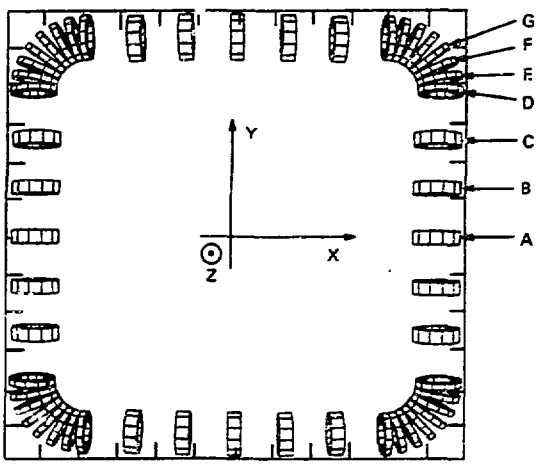

Fig. 1. Geometry of an EBS configuration indicating the coil arrangements (top view). Coordinate system used is shown (X and Y axes are indicated; Z axis points out of the viewing area). There are four symmetry planes and eight field periods. One field period is represented by coils A through G.

Numerically calculated transport coefficients indicate that the neoclassical confinement time should be a factor of 5 to 15 larger [depending on the global mirror ratio $M_G = B_{corner}/B_{side}$ (midplane)] for the EBS than for an EBT of comparable size. In order for neoclassical losses to be dominant, ripple-induced losses from the toroidal solenoid sections should be smaller than the neoclassical losses from the straight sections. The ripple is produced by the finiteness of

*Research sponsored by the Office of Fusion Energy, U.S. Department of Energy, under Contract No. DE-AC05-84OR21400 with Martin Marietta Energy Systems, Inc.

the number of coils in the corners. The presence of ripple will introduce additional particle trapping and, if large enough, may be the primary factor determining the transport of particles and energy in the region of low collision frequencies.[5] In the phenomenon known as ripple trapping, the particles become trapped in the field minimum between coils (between coils which produce the toroidal solenoid field in the corners) that are localized in the toroidal direction and experience a unidirectional toroidal drift that leads to the ripple diffusion. A similar phenomenon occurs in other toroidal configurations (e.g., tokamaks). In this paper we calculate the enhanced transport coefficients associated with the ripple-induced drifts and compare them with the EBT neoclassical diffusion coefficients to determine the allowable range for the magnitude of the field ripple.

In our examples, for an experimental-size device, we consider an EBS configuration (Fig. 1) whose sides are constructed from EBT-Scale (EBT-S) mirror coils (with five mirror coils per side, such as A, B, and C) and whose corners are 90° sections of a toroidal solenoid in which the field is produced by (1) four EBT-S mirror coils or (2) eight half-size EBT-S coils (such as D, E, F, and G) per corner.

FIELD ERROR CALCULATIONS

As pointed out, the field errors can arise from many different sources: coil misalignment, imperfect winding effects in a coil, magnetic fields from buswork and leads, and field perturbations due to the presence of magnetic materials. Although all these sources can cause significant error fields, we will discuss only the first error source in this paper.

The presence of field errors introduces an additional vertical drift of order $v_\parallel(\delta B/B)$ to the system.[4] Mirror-trapped particles ($v_\parallel/v \sim 0$) are not significantly affected (to lowest order) by field errors because their motion is restricted to a single sector.[3,4] The drift orbits of toroidally passing particles ($v_\parallel/v \sim 1$), on the other hand, are modified by this additional drift, which, if it is large enough, causes them to walk out of the confinement system. We define a critical error field $(\delta B/B)_{crit}$ such that if $(\delta B/B) > (\delta B/B)_{crit}$ the drift surfaces of toroidally passing particles become open. From the requirement of having closed drift surfaces,[3,4] it is necessary to have $(\delta B/B) < (\delta B/B)_{crit} \sim \rho_e/\langle R_c\rangle$, where ρ_e is the electron Larmor radius and $\langle R_c\rangle$ is the average magnetic radius of curvature. For an experimental-size device (a device similar in size to EBT-S), the required $(\delta B/B)_{crit} \sim$ few $\times 10^{-4}$, and for a reactor-like device $(\delta B/B)_{crit} \lesssim 10^{-5}$. We note that the field errors will be more critical in regions of large magnetic field and large radii of curvature $[(\delta B/B) \sim \rho/R_c \sim (BR_c)^{-1}]$, that is, near the coil throat and especially at the magnetic axis.[4] Thus, we will evaluate the amount of $\delta\vec{R}$ that a field line centered at the magnetic axis (starting in the coil throat) misses connecting with itself when followed once around the torus. For perfect coils installed with no misalignment, this number should be zero.

Numerical Calculations Due to Single-Coil Misalignment

Shown in Fig. 1 is the geometry of an EBS configuration indicating the coil arrangements and coordinate system used. An EBS configuration has four symmetry planes and eight field periods. Specific coils involved in the calculations within one field period are designated A through G in Fig. 1. Figure 2 shows magnetic field lines in the equatorial plane (X-Y plane) with specific dimensions. The mirror sector length (or the coil spacing) in the sides is $L_m \simeq 40$ cm, and the major radius of the corner sections is $R_{corner} \simeq 44$ cm, with the axis of each corner section displaced radially outward by $(\Delta\ \text{shift})_{corner} \simeq 2.5$ cm from the axis of the sides. This displacement and the length of the transition sector (L_{Tr}) are adjusted so that the rings in the transition sector (the sector connecting the simple mirror field to a $1/R$ varying toroidal field) form on the same flux lines as in the axisymmetric sectors. Depending on the ratio of the currents in the corner coils to the currents in the straight section, the transition sector length is typically larger (~2 to 4 cm) than the length of the mirror sectors. For $I_{corner}/I_{side} \simeq 1.2$–$1.4$, $L_{Tr} \simeq 42$–44 cm. In our example, we have $I_{corner}/I_{side} \simeq 1.4$ and $L_{Tr} \simeq 42$ cm.

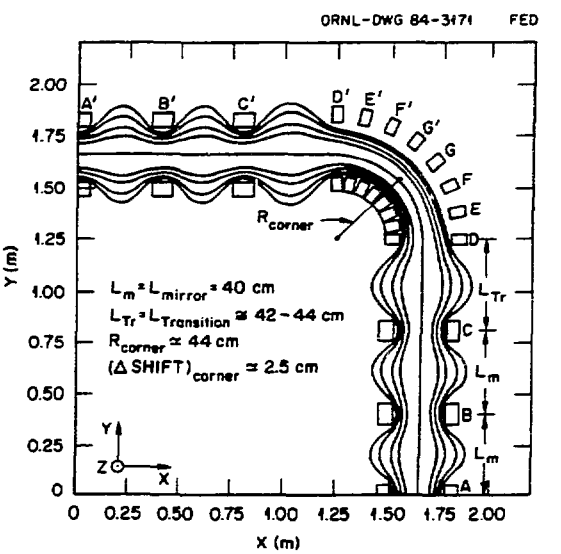

Fig. 2. Magnetic field lines in the equatorial plane (X-Y plane) of an EBS are shown for one quadrant. A through G coils and their mirror images G' through A' are shown along with specific dimensions used in the calculations. Here L_m = mirror sector length, L_{Tr} = transition sector length, R_{corner} = radius of the corner, and $(\Delta\text{shift})_{corner}$ = (center of coil D − center of coil A) = $X_{D0} - X_{A0}$.

The field line geometry shown in Fig. 2 is calculated with finite coil dimensions from EFFI, which do not differ from those of circular filament approximation.[2] The code evaluates $\delta\vec{R}(\delta X, \delta Y, \delta Z)$ in a coil plane by integrating the field line equations through one full period around the machine (360° in ϕ). Theoretically, $\delta\vec{R}$ vanishes for the ideal positions and orientations of the coils. Actual numerical results obtained from the code usually range from 10^{-9} to 10^{-10} cm for $|\delta\vec{R}|$. Therefore, the accuracy of the code seems sufficient for the purpose of the present study.

There are five degrees of freedom associated with each coil: three for the position of the coil center and two for the angles of the coil plane. The five corresponding coil errors are denoted by ΔX, ΔY, ΔZ, $\Delta\theta$, and $\Delta\phi$, where θ is the angle between the Z axis and the projection of the coil normal to the X-Y plane and ϕ is the angle between the coil plane (which is coplanar with the Z axis) and the X axis in the X-Y plane (Fig. 3).

Table I lists the field line displacement $\delta\vec{R}$ obtained with only one coil perturbed and with only the error involved in coil position or orientation. The field line displacement is measured in the center of the coil plane of the A coil (X-Z plane with coil center at $X = X_{A0}$, $Y = 0$, $Z = Z_{A0} = 0$). Figures 4 and 5 show the direction and relative magnitude of field line displacement in a circle with a radius of 11 cm (the radius of the clear bore under the coil) in the coil plane for $\Delta\theta = 1°$ and $\Delta\phi = 1°$, respectively.

The results of the calculations indicate that the field line closure is most sensitive to angular misalignment of the coils ($\Delta\theta$ and $\Delta\phi$). In these cases, an *assumed* angular error of 1° causes $\delta B/B \simeq 2.22 \times 10^{-4}$. We note that in EBT-S a similar angular misalignment of 1° ($\Delta\theta$ or $\Delta\phi$) causes similar error fields ($\delta B/B \simeq 2.22 \times 10^{-4}$). An important observation is that the effects of errors in θ and ϕ are essentially orthogonal: $\Delta\theta$ causes a vertical displacement of the field lines (Fig. 4) and $\Delta\phi$ causes a horizontal displacement of the field lines (Fig. 5). Errors in absolute positions are much less sensitive; a misalignment of 1 cm in one coil location yields an error $\delta B/B \sim 10^{-6}$ to 10^{-7} (Table I).

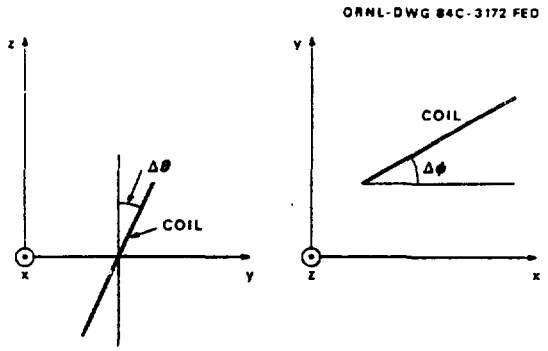

Fig. 3. Two angles of the coil plane. Orientations of X, Y, and Z coordinates are shown, with the same orientation as in Figs. 1 and 2.

Statistical Analysis of Errors

In the previous section, we determined that the dominant misalignment contributions to field errors were in the two angles θ and ϕ. Since the proper determination of angular

Table I. Results of perturbations to one coil*

Coil	Perturbation	Field line displacement ($\delta\vec{R}$) δX (mm)	δZ (mm)	$\delta B/B$
A	$\Delta\theta = 1°$	≈0	−2.82	2.22×10^{-4}
A	$\Delta\phi = 1°$	−2.81	≈0	2.22×10^{-4}
G	$\Delta\theta = 1°$	≈0	−1.17	9.22×10^{-5}
G	$\Delta\phi = 1°$	−1.21	0	9.54×10^{-5}
B	$\Delta X = 1$ cm	1.1×10^{-2}	0	8.67×10^{-7}
B	$\Delta Y = 1$ cm	6.2×10^{-3}	0	4.89×10^{-7}
B	$\Delta Z = 1$ cm	0	1.7×10^{-2}	1.34×10^{-6}
B	$\Delta I/I = 10^{-3}$	3.4×10^{-4}	0	2.68×10^{-8}

*Field line displacement is measured in the center of the A coil plane (X-Z plane). Calculated lack of field line closure $\delta\vec{R}(\delta X, \delta Z)$ and corresponding field error $\delta B/B = |\delta\vec{R}|/C$, where C is the circumference (field line length).

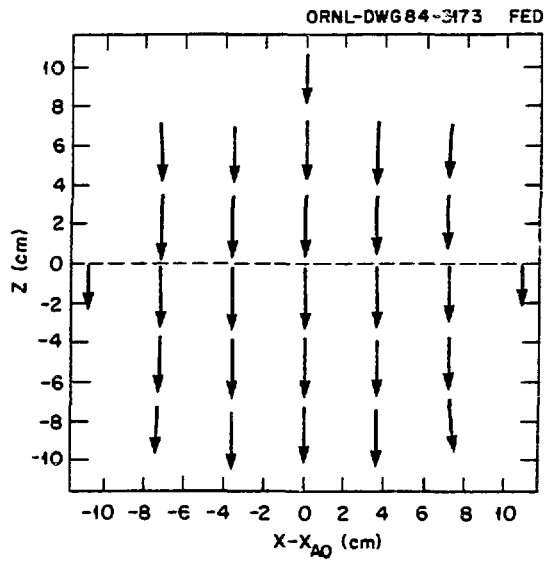

Fig. 4. Arrow plot showing the direction and relative magnitude of field line displacements in the plane of A coil for $\Delta\theta = 1°$. The largest magnitude is 2.82 mm at the coil center (0,0).

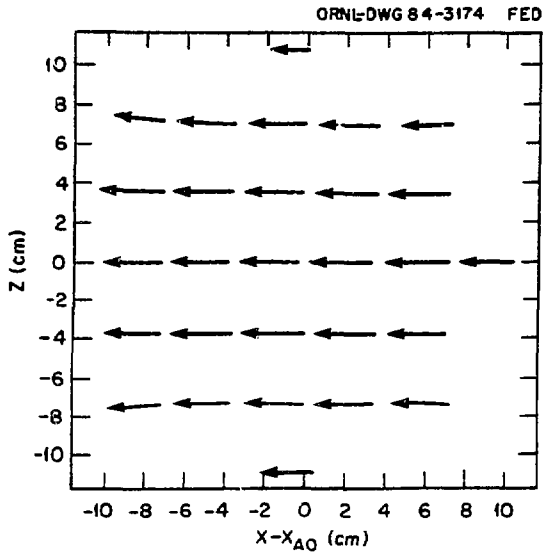

Fig. 5. Arrow plot showing the direction and relative magnitude of field line displacements in the plane of A coil for $\Delta\phi = 1°$. The largest magnitude is 2.81 mm at the coil center (0,0).

alignment will require fairly stringent positional alignment also, we discuss only the angular errors and assume that nonclosure of field lines arising from positioning errors is small relative to the angular ones.

First, we consider only the variations in θ. The total number of coils in the sides is $N_s = 20$ (five coils per side) and in corners $N_c = 32$ (eight coils per corner). For one coil (side or corner), we have the expression $\delta B/B = C_\theta \Delta\theta$. If we assume that the errors in all 20 straight-side coils are distributed normally with one Gaussian distribution and that the errors in all 32 corner coils are distributed normally with another Gaussian distribution (both of which have a mean error of zero and an rms error of θ_{rms}), then the problem is exactly equivalent to the one-dimensional random walk problem. Each magnet error $\Delta\theta$ contributes a step-size $(\delta Z)_j$ to a field line, where $j = s$(side), c(corner). For small individual displacements, the problem can be treated as a linear superposition of steps of varying size and direction with an rms step-size determined by θ_{rms}. For N steps, the rms displacement $\delta Z_N = N^{1/2}\,\delta Z_1$; then,

$$(\delta B/B)_\theta = (\delta B/B)_{corner} + (\delta B/B)_{side} ,$$

$$(\delta B/B)_{corner} = N_c^{1/2}(C_\theta \theta_{rms})_c ,$$

$$(\delta B/B)_{side} = N_s^{1/2}(C_\theta \theta_{rms})_s .$$

Thus,

$$(\delta B/B)_\theta = [(32)^{1/2}C_{\theta c} + (20)^{1/2}C_{\theta s}]\theta_{rms} ,$$

where $(\theta_{rms})_c = (\theta_{rms})_s$ is taken.

The same arguments apply for errors in the ϕ direction. Since the errors in ϕ and θ cause the same magnitude change in $\delta B/B$ (i.e., $C_\theta = C_\phi$, from Table I) but are perpendicular in direction, the expression for the total field error is simply

$$(\delta B/B) = [(\delta B/B)_\theta^2 + (\delta B/B)_\phi^2]^{1/2} ,$$

which yields

$$\delta B/B = [(32)^{1/2}C_{\theta c} + (20)^{1/2}C_{\theta s}](\theta_{rms}^2 + \phi_{rms}^2)^{1/2} ,$$

where ϕ_{rms} is the rms error in ϕ. The previous expression is valid if the errors in ϕ and θ are uncorrelated, which seems to be the most reasonable assumption to make. Finally, if we assume the rms errors in the ϕ and θ directions to be equal, then

$$\delta B/B = [8C_{\theta c} + (40)^{1/2}C_{\theta s}]\theta_{rms} .$$

From Table I we have $C_{\theta c} = 9.54 \times 10^{-5}$ and $C_{\theta s} = 2.22 \times 10^{-4}$. Thus, $\delta B/B = 2.17 \times 10^{-3}\,\theta_{rms}$, where θ_{rms} is expressed in degrees.

The question remains, "What is the inherent $\delta B/B$ that can be tolerated?" (That is, what is the field error inherent to the device construction *without global correction?*) In the EBT-S device the inherent field error was $\delta B/B \simeq 5 \times 10^{-4}$, which was corrected to a level of $\delta B/B \simeq 10^{-4}$ with the global field error correction coils.[3,4] That is, the global field correction coils correct 80% of the inherent device field error in EBT-S. Based on the EBT-S experience[4] and the fact that coil alignment errors produce fairly uniform field errors across the plasma (Figs. 4 and 5), we assume that similar levels of field errors ($\delta B/B \simeq 10^{-4}$) will be required in EBS and that the global field error correction coils can correct 80% of the inherent device field error. Thus, the inherent field error criterion (that is, five times that for the net field error $\delta B/B \simeq 5 \times 10^{-4}$) will yield the required values for θ_{rms}. Solving

$$\delta B/B = 2.17 \times 10^{-3}\theta_{rms} = 5 \times 10^{-4} ,$$

we have $\theta_{rms} = 0.23°$.

Since the treatment here is statistical in nature (as is the alignment of the coils), the actual $\delta B/B$ is not specified exactly by a specification of θ_{rms}. Rather, it has a Gaussian distribution; when corrected with global correction coils, the probability that $\delta B/B$ will be less than 10^{-4} is about 68% and the probability that it will be less than 2×10^{-4} is more than 95%.

Because drift orbits in EBS are much better centered than those in EBT-S,[1,2] the effect of field errors on particle orbit displacement might be expected to be more pronounced in EBS than in EBT-S. In this regard, if we choose to be more pessimistic in the field error criterion in EBS than in EBT-S, we can assume that the inherent field error should not exceed $\delta B/B \simeq 2 \times 10^{-4}$ (instead of $\delta B/B \simeq 5 \times 10^{-4}$). Under this pessimistic assumption θ_{rms} (pessimistic) $\simeq 0.1°$. With this value of θ_{rms}, the probability that inherent $\delta B/B$ will be less than 4×10^{-4} is greater than 95%, and, when it is corrected, $\delta B/B$ is less than 8×10^{-5}.

Repeating similar calculations for a typical EBS reactor,[2] we find $\delta B/B \simeq 1.7 \times 10^{-3}\theta_{rms}$. As noted earlier, $(\delta B/B)_{crit} \lesssim 10^{-5}$. Again, assuming that the intrinsic error criterion is five times that for the net error field, $\delta B/B \lesssim 4 \times 10^{-5}$. Thus, for a reactor, the θ_{rms} required to obtain this value of $\delta B/B$ is $\theta_{rms} \simeq 0.024°$.

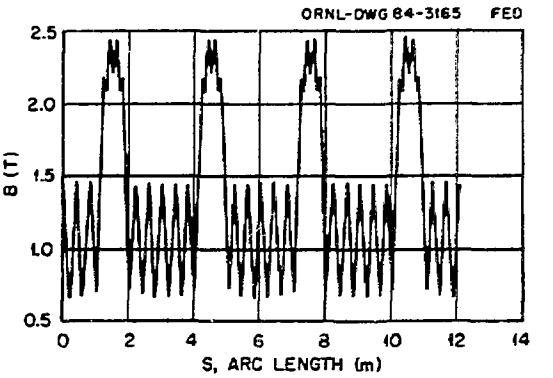

Fig. 6. Magnetic field strength as a function of arc length along the magnetic axis for a four-coil per corner EBS.

RIPPLE EFFECTS

In this section we consider the effect of toroidal field ripple (due to the discrete coils in the high-field corners) on transport. In the presence of ripple, there is a new class of so-called locally trapped particles ($v_\parallel/v \sim 0$) in the corners. These particles oscillate (trapped) in the field minimum (local magnetic well) between coils (those which produce the toroidal solenoid field in the corners) that are localized in the toroidal direction and experience a unidirectional toroidal drift that leads to the ripple-enhanced diffusion. Especially in the low-collisionality (ν/Ω) regime, ripple-induced losses could lead to significant increases in diffusion and thermal conductivity and may also be the main factor determining the transport of particles and energy. We note that the ripple trapping affects only a relatively small group of particles, that is, those with $v_\parallel$ (parallel velocity) so small that they can be trapped in the ripple.

In general, the ripple modulation δ (magnitude of field ripple) varies both radially and poloidally. The poloidal variation has the effect of reducing or completely eliminating the ripple well depth on the inside of the toroidal sections, with the precise degree of reduction depending on the shape of the coils and the position of the plasma within the coils.[5] For simplicity, we will neglect the poloidal variations, with the result of overestimating the ripple effects.

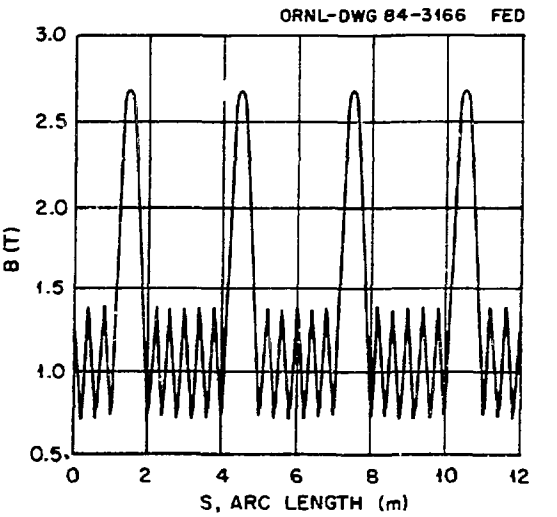

Fig. 7. Magnetic field strength as a function of arc length along the magnetic axis for an eight-coil per corner EBS (Fig. 2).

Magnetic Field Model

Figures 6 and 7 show the magnetic field strength as a function of arc length along the magnetic axis of a four- and eight-coil per corner EBS, respectively. The on-axis mirror ratio in the sides is seen to be 1.9, and the global mirror ratios [B_{corner}/B_{side} (midplane)] for these particular cases are 3.4 and 3.85, respectively. In both cases the corner coils have the same total number of ampere-turns. Although the field ripple is apparent for a four-coil per corner case (Fig. 6), the ripple is practically zero for most of the plasma cross section for an eight-coil per corner case (Figs. 2 and 7). A variation of field ripple as a function of normalized radius is shown in Fig. 8 for both cases and is summarized in Table II.

For high-field toroidal corners, a simple model for the magnetic field is

$$\vec{B} = \frac{B_o}{1 + \epsilon \cos\theta}\left[\frac{B_r}{B_\phi}\ ,\ 0\ ,\ 1 - \delta(r,\theta)\cos N\phi\right] ,$$

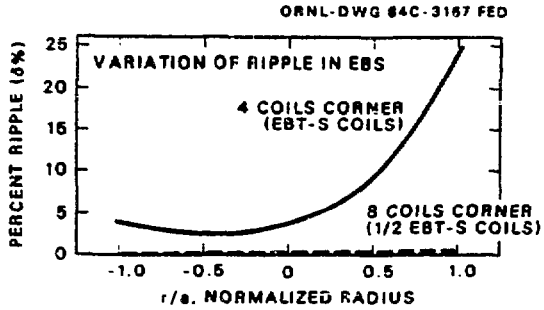

Fig. 8. Variation of ripple amplitude δ as a function of radius for (a) four coils per corner (solid line) and (b) eight coils per corner (dashed line).

Table II. Ripple variation in the corners of EBS

Normalized radius[a] r/a	Ripple amplitudes (%) Four-coil/ corner	Eight-coil/ corner
−1.0	3.5	0
−0.5	2.5	0
0.0	4.0	0
+0.5	8.5	~0
+1.0	~25.0	~0.5

[a]Here a is the last field line that just grazes the coil throat in the straight sections ($a \simeq 11$ cm).

where r and θ are polar coordinates in the minor cross section of the corners, ϕ is the angular coordinate (toroidal angle) along the magnetic axis of the corners, $\epsilon = r/R_o$ is the inverse aspect ratio of the toroidal corner (with R_o the major radius of the corner), N is the number of coils in the corners (a four-coil per corner case corresponds to an $N = 12$ coil torus and an eight-coil per corner case corresponds to an $N = 28$ coil torus), and $\delta(r,\theta)$ is the ripple well depth (modulation), defined as

$$\delta(r,\theta) = \left(\frac{B_{max} - B_{min}}{B_{max} + B_{min}}\right)_{corner} \simeq \left(\frac{\Delta B}{B_o}\right)_{corner} .$$

The radial component of $\vec{B}$, necessary to satisfy $\vec{\nabla} \cdot \vec{B} = 0$, is small (on the order of $B_r \sim \delta B_o \sin N\phi$). Thus, the field strength in the corner is approximately

$$B \simeq B_\phi \simeq B_o[1 - \epsilon \cos\theta - \delta(r,\theta)\cos N\phi] .$$

Threshold and Critical Energies (Ref. 5)

The threshold energy is defined as the energy above which particles execute more than one bounce motion in a ripple before being scattered out of the loss region ($v_\parallel < \delta^{1/2} v_\perp$) associated with ripples (Fig. 9). This energy can be obtained by setting τ_{eff}(scattering) = τ(bounce) or ν_{eff}(scattering) = ν(bounce), where $\nu_{eff} = \nu_{90}/(\Delta\theta)^2 = \nu_{90}/\delta$ and ν(bounce) = $\delta^{1/2} v/L = \delta^{1/2} vN/(2\pi R_o)$. Here ν_{90} is the 90° collision frequency, v is the particle speed, L is the length of the ripple well ($L = 2\pi R_o/N$), and the fraction of particles that are ripple trapped is equal to $(\delta)^{1/2}$. Combining all gives the threshold energy (temperature) as (in mks units with temperature in electron-volts)

$$T_{th} \simeq 90\delta^{-3/4}(R_o/N)^{1/2}(10^{-20} n_e)^{1/2} \quad \text{(eV)} .$$

For the four-coil per corner case, considering plasmas with *mid-*10^{18} m^{-3} density and $R_o \simeq 0.4$ m, the threshold energy is about 30 eV (10 eV) at the plasma center (edge). For the eight-coil per corner case, $T_{th} \simeq 125$ eV at the plasma edge and is several orders of magnitude larger at the plasma center.

The critical energy is defined as the energy above which particles will reach the wall if they are trapped in the ripple. When a particle is trapped in a ripple ($T > T_{th}$), its guiding center drifts along a contour of constant B. Because mod-B contours are not closed in a toroidal field, the particles are not confined unless they are scattered out of the ripple loss region before they can reach the wall. Thus, the critical energy can be determined by setting τ_{eff}(scattering) = τ(drift) = a/v_{drift}, where $v_{drift} \simeq T/eBR_o$. For ions, this gives a critical energy (in mks units with T in electron-volts) of

$$T_{c,i} \simeq 1.6 \times 10^3 (BR_o a/\delta)^{2/5}(10^{-20} n_e)^{2/5} \quad \text{(eV)} .$$

The critical energy is a factor of $(m_i/m_e)^{1/5}$ (≃4.5 for a hydrogen plasma) larger for electrons. Again, considering the four-coil per corner case, $T_{c,i}(r = 0) \simeq 600$ eV and $T_{c,i}(r = a) \simeq 250$ eV. Corresponding electron temperatures are higher (by a factor of ~4.5). For an eight-coil per corner case, $T_{c,i}(r = a) \simeq 1.5$ keV and $T_{c,i}(r = 0) >> T_{c,i}(r = a)$.

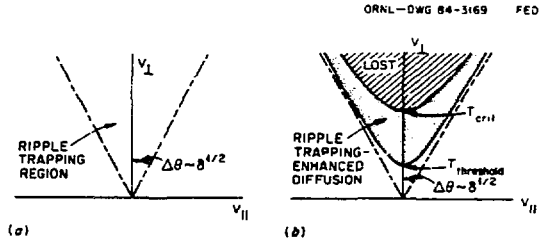

Fig. 9. (a) Ripple loss region and (b) critical energies.

The critical energy previously defined is for a zero electric field. In the presence of a finite electric field, if the particles are trapped in the ripple and if their energy exceeds $T_*(T > T_*)$, the particle orbits are not necessarily open because of the $\vec{E} \times \vec{B}$ precessional drift, which balances the vertical (toroidal) drift.[2] The shift in particle drift orbits is $\Delta x = v_{drift}/\Omega$, where $r\Omega \sim (T/eBR_c) + (E/B)$ is the poloidal drift velocity with $R_c = -(\partial \ln B/\partial r)^{-1}$. For particle orbits to be closed, $\Delta x \leq a/2$, or, conversely, for particles trapped in the ripple to drift to the wall, $\Delta x \geq a/2$. Combining all gives a critical energy in the presence of an electric field above which particles will reach the wall:

$$T_{*\mathcal{L}} \geq \left[\frac{eEa}{r}\right]\left[\left(\frac{1}{R_o}\right) - \left(\frac{a}{rR_c}\right)\right]^{-1} .$$

For weak ripples, rR_c in the corner is very large (approaches infinity). With approximately $E = \Delta\phi/\ell_E$, where ℓ_E is the electric field scale length (which is on the order of plasma radius), we have

$$T_{*E} \geq (a/\ell_E)(R_c/a)\Delta\phi \simeq \Delta\phi/\epsilon .$$

Here ϵ is the inverse aspect ratio ($\epsilon \sim 1/3$–$1/5$). Thus, only if $T_{*E} \gtrsim (3\text{–}5)\Delta\phi$ will particles be directly lost. Combining all, we define

$$T_{crit,i} = \max(T_{*,i}; T_{*E}) ,$$

$$T_{crit,e} = \max(T_{*,e}; T_{*E}) .$$

Ripple-Enhanced Diffusion—Simple Estimates

From the critical energies (T_{th}, T_{crit}) defined earlier, we can see that the ripple collisionality regime can be divided into three regions (Fig. 10). The upper collision frequency point ($\nu > \nu N\delta^{3/2}/R_o$), above which transport losses diminish to zero, is the point at which the plasma particle temperature decreases below the threshold energy ($T < T_{th}$). In the middle range of the collisionality regime ($\rho\nu\delta/Ra < \nu < \nu N\delta^{3/2}/R_o$, where ρ is the gyroradius), transport coefficients scale as ν^{-1} because the particles are scattered out of the loss region before they can drift out of the device. To convey the spirit of simple diffusion estimates, we give a rough picture of the random walk process.

The average step-size taken by a ripple-trapped particle is $(\Delta x)^\delta \sim v_{drift} \cdot \tau^\delta_{eff} = v_{drift} \cdot (\delta/\nu_{90})$. The frequency with which such steps are taken is $\nu^\delta_{eff} = \nu_{90}/\delta$. The fraction of particles participating in this ripple trapping is $f^\delta = \delta^{1/2}$. Thus, the diffusion coefficient associated with ripple trapping is

$$D^\delta \sim [(\Delta x)^\delta]^2 \cdot \nu^\delta_{eff} \cdot f^\delta \sim \delta^{3/2} v^2_{drift}/\nu_{90} .$$

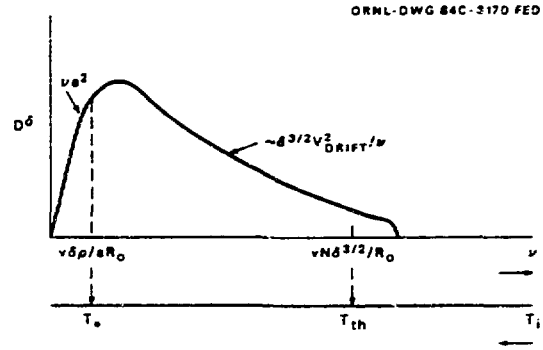

Fig. 10. Ripple collisionality regime.

Finally, in the absence of electric fields, at very low collision frequencies ($\nu < \rho\nu\delta/R_o a$), the particle temperature increases above the critical energy, and all particles trapped in the ripples will drift to the wall without being scattered out of the loss region. The corresponding diffusion coefficient is $D \sim \nu_{90} a^2$.

Comparison with Neoclassical Losses

Here we compare the ripple-enhanced diffusion coefficients with the conventional EBT neoclassical diffusion coefficients to determine the allowable range for the magnitude of the field modulations (ripples). The neoclassical diffusion coefficient for EBT is given by

$$D^{NC} \sim (\Delta x)^2[\nu/(1 + \nu^2/\Omega^2)] ,$$

where $\Delta x = v_{drift}/\Omega$ and $\nu = \nu_{90}$. In the collisionless regime ($\nu/\Omega \ll 1$),

$$D^{NC} \sim \nu_{90}(\Delta x)^2 \sim \nu_{90}(v_{drift}/\Omega)^2 .$$

In order for $D^\delta < D^{NC}$, that is,

$$\delta^{3/2} v^2_{drift}/\nu_{90} < \nu_{90}(v_{drift}/\Omega)^2 ,$$

we find $\delta^{3/2} < (\nu/\Omega)^2$ or $\delta < (\nu/\Omega)^{4/3}$. For $\nu/\Omega \sim 0.1$, representative of present-day experiments, the magnitude of the ripple well depth should be $\delta < 4.5\%$ in order for ripple losses not to be dominant. For very low collision frequencies ($\nu/\Omega \sim 0.01$, representative of reactor-like plasmas), one requires $\delta < 0.5\%$. We see from this example that for the four-coil per corner case the ripple losses will dominate. However, for the eight-coil per corner case the overall enhanced losses due to ripple will have a negligible effect on plasma confinement.

We note that the estimates given here for ripple magnitudes are somewhat pessimistic due to neglect of (1) the effect of poloidal variations in ripple magnitude and (2) the influence of the ambipolar electric field, both of which play an important role.

ACKNOWLEDGMENT

The authors would like to thank D. K. Lee for help in numerical calculations for field errors and in generating Figs. 4 and 5.

REFERENCES

1. L. W. OWEN, D. K. LEE, and C. L. HEDRICK, "ELMO Bumpy Square," in *Advanced Bumpy Torus Concepts—Proceedings of the Workshop*, CONF-830758, Oak Ridge National Laboratory (1983).
2. N. A. UCKAN et al., "ELMO Bumpy Square," ORNL/TM-9110, Oak Ridge National Laboratory (1984).
3. T. UCKAN et al., "Field Errors in EBT and Their Effects on the Ambipolar Potential," ORNL/TM-7912, Oak Ridge National Laboratory (1981); T. UCKAN, "Field Error Measurements on EBT," *Bull. Am. Phys. Soc.* **27**, 1115 (1982).
4. T. UCKAN, "Inherent Magnetic Field Error Measurements in ELMO Bumpy Torus," *Rev. Sci. Instrum.* **56**, (1985).
5. N. A. UCKAN et al., "Effects of the Poloidal Variation of the Magnetic Field Ripple on Enhanced Heat Transport in Tokamaks," ORNL/TM-5438, Oak Ridge National Laboratory (1976).